S04130200-DDD10000-R00

SECOND TARGET STATION (STS) PROJECT

The Suitability of Compact Neutron Moderators for the Initial Suite of STS Instruments

John F. Ankner, Yaohua Liu, and Shuo Qian

March 2024

OAK RIDGE NATIONAL LABORATORY
MANAGED BY UT-BATTELLE FOR THE US DEPARTMENT OF ENERGY

S04130200-DDD10000-R00

SECOND TARGET STATION (STS) PROJECT

THE SUITABILITY OF COMPACT NEUTRON MODERATORS FOR THE INITIAL SUITE OF STS INSTRUMENTS

John F. Ankner, Yaohua Liu, and Shuo Qian

March 2024

Prepared by
OAK RIDGE NATIONAL LABORATORY
Oak Ridge, TN 37831-6283
managed by
UT-BATTELLE, LLC
for the
US DEPARTMENT OF ENERGY
under contract DE-AC05-00OR22725

Approvals

Document Title		ISSUE DATE: March 25, 2024
PREPARED BY John F. Ankner	PROJECT Second Target Station	DOCUMENT NUMBER: S04130200-DDD10000

	Signature / Date					
	Rev. 00	Date	Rev. 01	Date	Rev. 02	Date
Instrument Scientist	John F. Ankner	3/25/24				
	John F. Ankner Digitally signed by John F. Ankner Date: 2024.03.25 15:01:13 -04'00'					
Instrument Systems Science Lead	Saurabh Kabra	3/25/24				
	Kabra, Saurabh Digitally signed by Kabra, Saurabh Date: 2024.03.25 15:13:51 -04'00'					
Instrument Systems Manager	Leighton Coates	3/25/24				
	Leighton Coates Digitally signed by Leighton Coates Date: 2024.03.26 09:49:44 -04'00'					

Revision	Description
00	Initial Release

ABSTRACT

The scientific productivity of neutron instruments depends on efficient use of the flux generated by neutron sources. A study of potential neutron moderators for the Spallation Neutron Source (SNS) Second Target Station (STS) [Gallmeier2016] determined that smaller moderators yield the brightest neutron sources, and a preliminary decision was made to deploy moderators of 30 mm dimensions at STS (in contrast with the 100×120 mm^2 moderators deployed at the SNS First Target Station). This document assesses the suitability of such compact moderators for the initial suite of STS instruments approved for construction in the project.

1. SAMPLE ILLUMINATION, PHASE SPACE, AND ACCEPTANCE

The simplest illumination of a sample by a neutron source (moderator) consists of the two separated by empty space. Consider a neutron moderator of height h_{m} illuminating a sample of height h_{s} located a distance L_{ms} from the moderator (Fig. 1A). No neutron can emerge from beyond the moderator and only neutrons that strike the sample are of use. The bounding paths of neutrons that strike the sample are labeled (1)-(4). These paths correspond to coordinates in a plot of neutron angular deviation γ_y vs. position y (Fig. 1B). The vertices of the parallelogram in (y, γ_y) coordinates are:

(1) $\left({h_{\mathrm{s}}}/{2}, \tan^{-1} {(h_{\mathrm{m}} + h_{\mathrm{s}})}/{2L_{\mathrm{ms}}}\right)$
(2) $\left(-{h_{\mathrm{s}}}/{2}, \tan^{-1} {(h_{\mathrm{m}} - h_{\mathrm{s}})}/{2L_{\mathrm{ms}}}\right)$
(3) $\left(-{h_{\mathrm{s}}}/{2}, -\tan^{-1} {(h_{\mathrm{m}} + h_{\mathrm{s}})}/{2L_{\mathrm{ms}}}\right)$
(4) $\left({h_{\mathrm{s}}}/{2}, -\tan^{-1} {(h_{\mathrm{m}} - h_{\mathrm{s}})}/{2L_{\mathrm{ms}}}\right)$.

Only neutrons with spatial and angular divergence coordinates within the gray shaded polygon strike the sample. The numbered paths in Fig. 1A correspond to the numbered vertices of the parallelogram in Fig. 1B. The polygon boundaries may be specified by the following sequence of operations on Fig. 1A: scan $h_{\mathrm{s}}/2$ to $-h_{\mathrm{s}}/2$ by rotating ray (1) to ray (2) about their intersection at $-h_{\mathrm{m}}/2$; next sweep from $-h_{\mathrm{m}}/2$ to $h_{\mathrm{m}}/2$ by rotating from ray (2) to ray (3); then, sweep from $-h_{\mathrm{s}}/2$ to $h_{\mathrm{s}}/2$ by rotating ray (3) to ray (4); finally, sweep from $h_{\mathrm{m}}/2$ to $-h_{\mathrm{m}}/2$ by rotating ray (4) to ray (1). The phase-space plot depicted in Fig. 1B is known as an acceptance diagram.

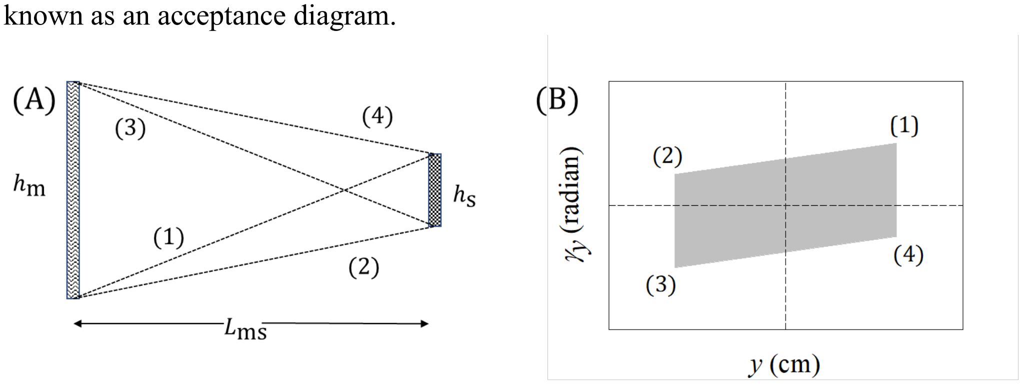

Figure 1: (A) The extremum paths from moderator (height h_{m}) to sample (height h_{s}) are labeled (1)-(4). (B) The extremum paths bound the angular divergence and spatial coordinates of neutrons able to travel a distance L_{ms} from the moderator and hit the sample. The numbered vertices of the polygon correspond to paths (1)-(4) on the schematic drawing.

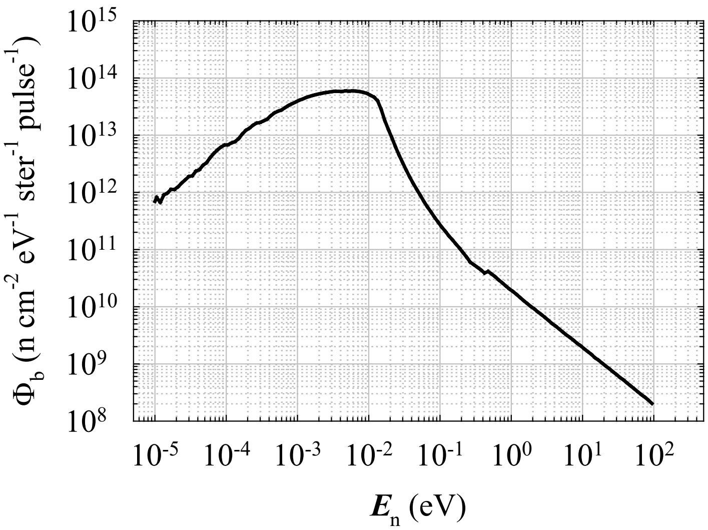

Figure 2: Brightness spectrum of a coupled supercritical H_2 STS moderator at 20 K with 700 kW proton power deposited on target.

The number of neutrons incident on the sample can be calculated if one knows the brightness of the moderator. Moderator brightness may be estimated using Monte Carlo methods (MCNPX) [Gallmeier2016] and broadly follows the blackbody emission of an object at the temperature of the moderator. Figure 2 shows brightness as a function of neutron energy for a proposed 3-cm-diameter cylindrical coupled 20 K H_2 moderator at STS illuminated by 700 kW of proton power deposited on target at 15 Hz. Such a plot assumes moderator emission to be isotropic in angle γ_y and position y on the moderator surface. This approximation is broadly valid in practice since instruments are constructed nearly "face-on" with moderators and divergence angles are small. Under these assumptions, neutron intensity on sample may be written [Zhao2013]:

$$I(E_\mathrm{n}) = \Phi_\mathrm{b}(E_\mathrm{n}) \int A(x, y, \gamma_x, \gamma_y, E_\mathrm{n})\, dx\, dy\, d\gamma_x\, d\gamma_y, \tag{1}$$

where E_n is neutron energy, Φ_b source brightness, x and γ_x are the horizontal position and angular divergence, respectively, of a neutron incident on the sample, orthogonal to the y coordinates defined above. The acceptance function A comprises the coordinates of neutrons emitted by the moderator capable of striking the sample.

The "instrument" depicted in Fig. 1 provides a simple application of the concept of acceptance. The area of the polygon in Fig. 1B is

$$\begin{aligned} A_y &= h_\mathrm{s}\left(\tan^{-1}\frac{h_\mathrm{m}+h_\mathrm{s}}{2L_\mathrm{ms}} + \tan^{-1}\frac{h_\mathrm{m}-h_\mathrm{s}}{2L_\mathrm{ms}}\right) \\ &\approx h_\mathrm{s}\left(\frac{h_\mathrm{m}+h_\mathrm{s}}{2L_\mathrm{ms}} + \frac{h_\mathrm{m}-h_\mathrm{s}}{2L_\mathrm{ms}}\right) = \frac{h_\mathrm{m}h_\mathrm{s}}{L_\mathrm{ms}} \end{aligned}, \tag{2}$$

where the divergence angles are assumed small. A similar expression for A_x may be derived for the sample and moderator widths w_s and w_m so that

$$I(E_\mathrm{n}) = \Phi_\mathrm{b}(E_\mathrm{n})A_xA_y = \Phi_\mathrm{b}(E_\mathrm{n})\frac{w_\mathrm{m}h_\mathrm{m}w_\mathrm{s}h_\mathrm{s}}{L_\mathrm{ms}^2} = \Phi_\mathrm{b}(E_\mathrm{n}) \times w_\mathrm{s}\frac{w_\mathrm{m}}{L_\mathrm{ms}} \times h_\mathrm{s}\frac{h_\mathrm{m}}{L_\mathrm{ms}}. \quad (3)$$

The geometrical character of acceptance is revealed explicitly by this simple example. Intensity depends only on the product of source brightness and independent horizontal and vertical acceptances. The acceptances in turn are just the product of the moderator and sample areas divided by the distance between moderator and sample squared. The final equality in Eqn. 3, though, is the most useful for general application of acceptance. In this form, neutron intensity I [n pulse^{-1}] at a given energy E_n is the product of source brightness at that energy Φ_b [n cm^{-2} steradian^{-1} pulse^{-1}] with the enclosed areas A_x [cm radian] and A_y [cm radian] of the acceptance diagrams (Fig. 1B). In addition, the assumption of isotropic moderator emission eliminates any geometrical character from the brightness more generally so that it acts as a simple multiplicative factor applied to the spatial and angular integrations in Eqn. 1. Acceptance can be propagated analytically [Carpenter1982] through rectilinear energy-dependent beamline components (e.g., reflecting guides) and its progress tracked through an instrument to design quite sophisticated neutron transport systems. Beam transport utilizing focusing optics or which otherwise scrambles x and y acceptance contributions can be handled using Monte Carlo methods and generalized acceptance via Eqn. 1.

2. THE QUITE INTENSE KINETICS REFLECTOMETER (QIKR)

To illustrate the effect of moderator size on instrument performance, we'll apply the acceptance framework to the QIKR instrument. This treatment will serve as a proxy for the other instruments being designed for the STS.

2.1 SPECIFYING ILLUMINATION

A challenge faced in instrument design is that natural collimation (Fig. 1) is smaller than could be tolerated in most instances. Since neutrons always and everywhere are scarce, trading resolution (divergence) for intensity is generally desirable. An important goal of the instrument designer, then, is to transport sufficient angular divergence to the sample to maximize intensity without unduly compromising resolution. Wishy-washy terms like "unduly" reveal a certain degree of subjectivity in this assessment. Does one optimize for an extreme (e.g., large) sample or for a typical sample? The ultimate decision depends on an intrinsically imprecise assessment of the future scientific needs of the community served by the instrument.

As one might expect from the name, QIKR will be a general-purpose neutron reflectometer and serve a scientific community with a broad range of needs and interests. Details of the QIKR concept may be found in a recent publication [Ankner2023]. A reflectometer must deliver a well collimated and spatially constrained beam onto a sample surface at a well defined (small) angle of incidence. The neutrons reflected from the surface are subsequently collected in a downstream detector. The incident beam is defined by upstream (s_u) and downstream (s_d) slits from a broader and more divergent beam delivered from the moderator by the neutron optical system (Fig. 3). The slit values s_u and s_d are defined by the desired beam footprint F and angular relative resolution $\delta\theta/\theta$. One can calculate the dependences using a little geometry and algebra,

$$s_\mathrm{u} \approx l_\mathrm{ud}\theta(\delta\theta/\theta), \quad (4)$$

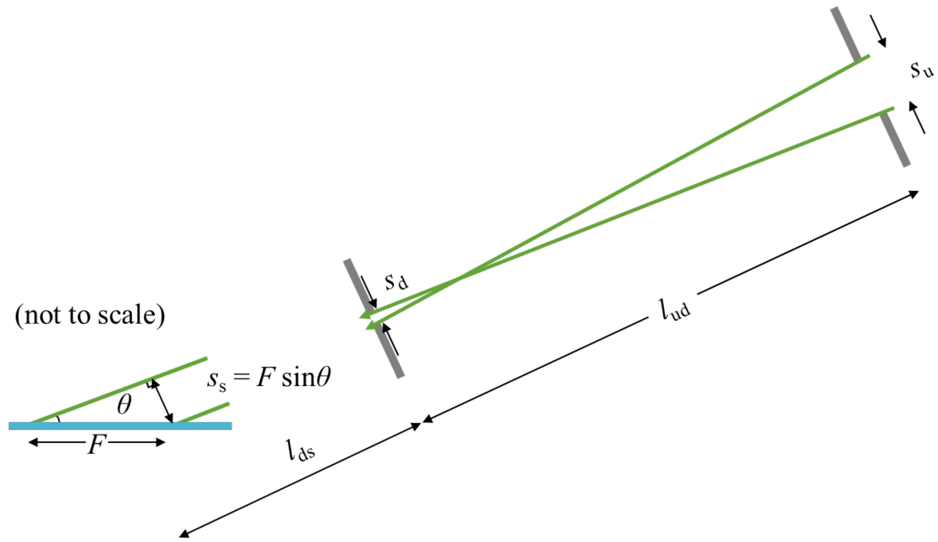

Figure 3: Collimation geometry for reflectometry. The neutron beam (green) is collimated by upstream and downstream slits, s_{u} and s_{d}, a distance l_{ud} apart, passing onto a sample a distance l_{ds} from the downstream slit. The beam strikes the sample at an angle θ (generally <5°). Specifying a given footprint F and angular resolution $\delta\theta/\theta$ determines the slit values [Ankner2023].

$$s_{\mathrm{d}} \approx \frac{l_{\mathrm{ud}}\theta[F - l_{\mathrm{ds}}(\delta\theta/\theta)]}{l_{\mathrm{ud}} + l_{\mathrm{ds}}}. \tag{5}$$

The two slits may be treated with the acceptance formalism presented in Fig. 1 and adjacent text. The integrated acceptance of the slits is given by the area of the corresponding parallelogram to that shown in Fig. 1,

$$\int A_y dy d\gamma_y \approx \frac{s_{\mathrm{u}} s_{\mathrm{d}}}{l_{\mathrm{ud}}}. \tag{6}$$

In Fig. 4, we've plotted the values (top) and integrated acceptances (bottom) of a series of apertures for the QIKR slit system illuminating an $F = 30$ mm footprint for a beam incident at $\theta = 2.5°$ onto a sample surface, a common configuration. Note that the integrated acceptance increases monotonically but sub-linearly with increasing $\delta\theta/\theta$ due to the gradual reduction of s_{d} needed to constrain the beam footprint. This increase of integrated acceptance with increasing $\delta\theta/\theta$ is the phenomenon that enables one to trade resolution for intensity.

2.2 RESOLUTION REQUIRED FOR SCIENCE

The specific experiments to be performed will dictate the required resolution and to what degree it might be relaxed to increase beam intensity via increased slit acceptance. Translating this non-specific statement into instrument specifications requires that we anticipate the experiments users will be

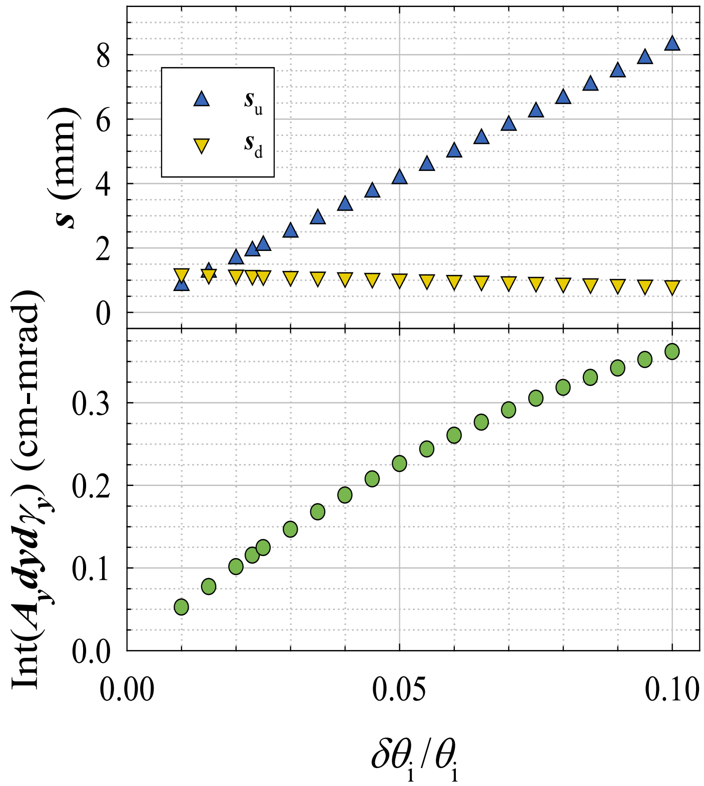

Figure 4: (top) Required apertures upstream (s_u) and downstream (s_d) for a beam incident onto a sample at θ_i = 2.5° painting an F = 3 cm footprint when l_{ud} = 190 cm and l_{ds} = 10 cm at different values of relative angular resolution $\delta\theta/\theta$ per Eqns. 4 and 5 in the main text. (bottom) Integrated acceptance for those slit settings per Eqn. 6 in the main text.

performing on QIKR. The scientific interests of the QIKR user community may be divided broadly into three categories: soft matter, energy materials, and biology [Ankner2023]. Despite the diverse array of materials of interest and sample environments needed to perform measurements within and between these three areas, the samples studied exhibit broadly similar structural characteristics. Soft matter samples typically consist of a mixture of deuterated and non-deuterated polymer layers ranging from 50-1000 Å in thickness [Aliakseyeu2023]; energy materials, such as battery electrodes, often include metallic layers several hundred Angstroms thick atop which electrochemically active films are deposited [Browning2019]; and much biological research involves the study of 20-50-Å-thick cell membrane analogs [Phan2020].

The instrumental resolution required to extract information from reflectivity measurements of these samples is determined by the thicknesses of the reflecting layers within them [Ankner1992]. The momentum transferred to a neutron reflected from a surface depends on its angle of incidence θ onto the surface and its wavelength λ,

$$\Delta p = \hbar Q = \hbar \frac{4\pi \sin\theta}{\lambda}, \tag{7}$$

where h is Planck's constant and Q the wavevector change in the scattering event. Figure 5 shows the specular reflectivity R multiplied by Q^4 plotted vs. Q for characteristic soft matter, energy, and biology

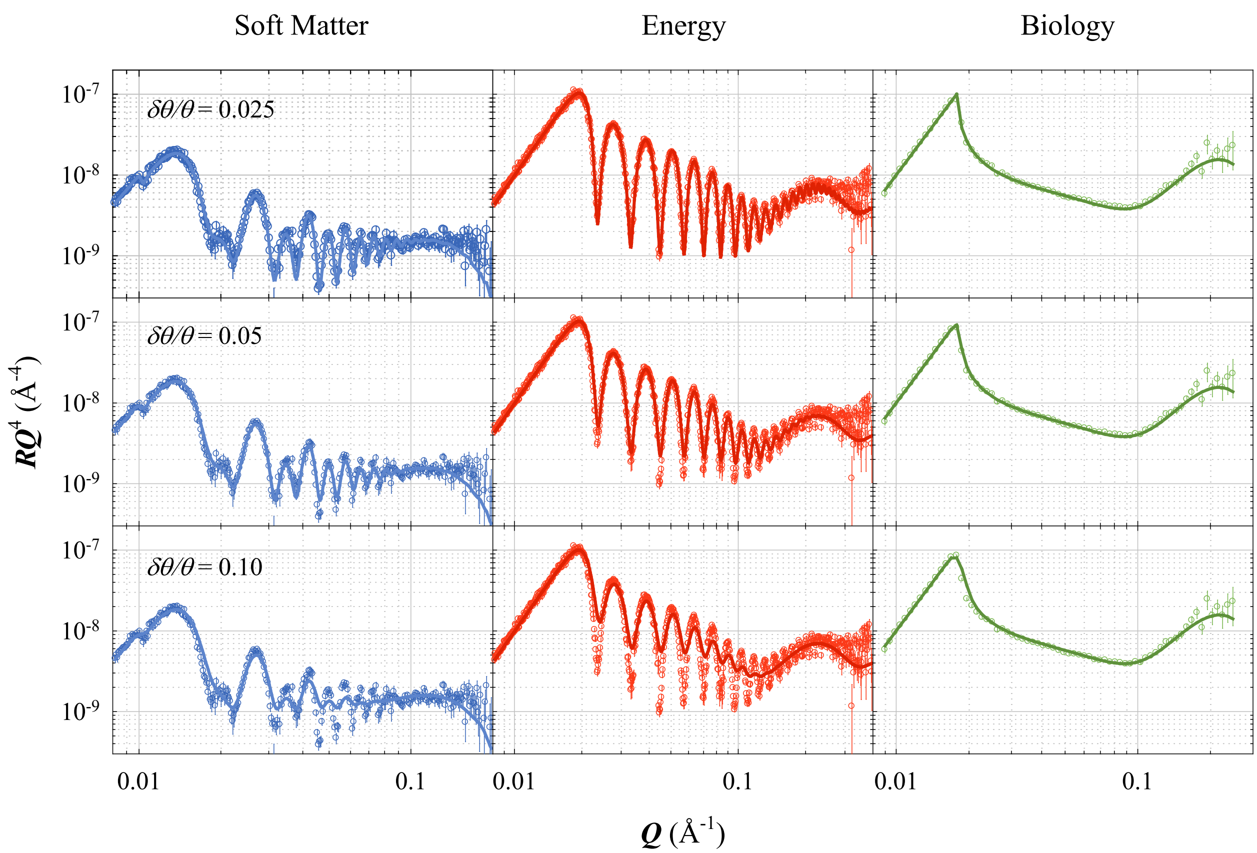

Figure 5: Measured specular reflectivity and fits at three different relative resolutions for characteristic samples in soft matter, energy materials, and biology.

samples. The data were fitted at three different relative resolutions, $\delta\theta/\theta = 0.025$, 0.05, and 0.1. Features in a specular reflectivity profile generally oscillate at frequencies given by the inverse of characteristic reflecting layer thicknesses – $\Delta Q \sim 2\pi/d$ (reciprocal space) so the instrumental resolution δQ needed to see these structures will be dictated by their size. Resolution can only be traded for intensity if doing so does not affect the quality of the information extracted from the data. In Fig. 5, the relatively thick (>100 Å) layers characteristic of polymer and battery electrode films produce high frequency oscillations requiring tight angular resolution to measure properly. Failure of the model fits (solid lines) to track the data are apparent even at $\delta\theta/\theta = 0.05$, worsening at higher Q values. For this reason, the default resolution for such measurements is $\delta\theta/\theta = 0.025$. Only the amphiphilic monolayer measured in the biology example can meaningfully benefit from the added intensity afforded by relaxed resolution without compromising the experiment. Currently at the First Target Station Liquids Reflectometer, fewer than 10% of the experiments performed look like the biology example. The overwhelming majority of experiments require finer resolution. For this reason, QIKR has been optimized for high resolution.

2.3 EFFECT OF MODERATOR SIZE ON PERFORMANCE

Considering the simple acceptance treatment depicted in Fig. 1 one can see that, purely based on acceptance, the larger moderator will always win. The larger moderator provides a geometrically greater range of neutron trajectories, so the only way a smaller moderator can outperform a larger one is by being

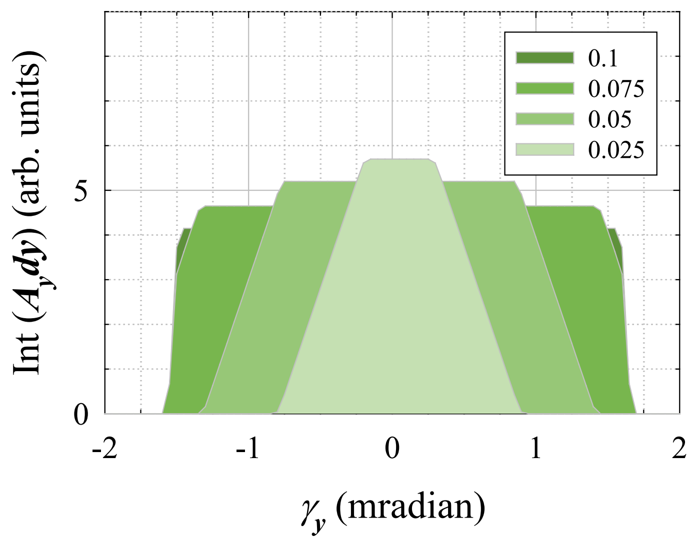

Figure 6: Vertical coordinate acceptance rocking curves for the QIKR-L central beam with slits illuminating an F = 30 mm footprint for relative resolutions ranging from $0.025 < \delta\theta/\theta < 0.10$ (l_{ud} = 190 cm, l_{ds} =10 cm).

brighter. This was indeed shown to be the case for the moderators simulated in [Gallmeier2016]. Table I from that work shows at factor of 3.94/2.74 = 1.44 increase in brightness for a 30×30 mm^2 versus a 50×50 mm^2 moderator. Is this factor great enough to overcome the geometrical advantage of the larger moderator?

The acceptance of the slits plotted in Fig. 4 may be viewed as a request to the upstream beamline optics and neutron source. Can the optics and neutron source fulfill that request? Consistent with the discussion of scientific needs in Section 2.2, QIKR, viewing a 30×30 mm^2 moderator, has been optimized so that the neutron guide system transports all neutron trajectories needed for operation in a relative resolution range $0.02 < \delta\theta/\theta < 0.07$ [Ankner2023]. Integrating over the spatial coordinate in Fig. 1B yields an instrumental rocking curve with a trapezoidal profile. Figure 6 depicts a series of these rocking curves for QIKR. For $\delta\theta/\theta > 0.07$, the trapezoid's left and right edges are truncated, indicative of insufficient angular divergence in the beam incident on the upstream slit to supply all the requested phase space volume. The absence of these neutron trajectories is a direct consequence of the limited view afforded by the small (30×30 mm^2) moderator. A larger moderator (e.g., 50×50 mm^2) could supply these trajectories and so eventually outperform the smaller, brighter moderator for more divergent beams. The larger moderator cannot, however, supply any additional trajectories for $\delta\theta/\theta < 0.07$ so the brighter smaller moderator wins. Since the bulk of the experiments are expected to be carried out at these tight resolutions, the smaller moderator yields better performance.

3. PIONEER, A SINGLE CRYSTAL DIFFRACTOMETER AND MORE

Next, we use the PIONEER diffractometer as a second case to investigate the optimal moderator size for STS instruments. Then, we expand the discussion to VERDI and CHESS, two instruments using guide systems like PIONEER. Based on the methodology developed by Konik and Ioffe [Konik2023], which combines analytical approaches with Monte Carlo simulations, we aim to determine the ideal moderator size per the science requirements without necessitating detailed knowledge of the deployed guide. The

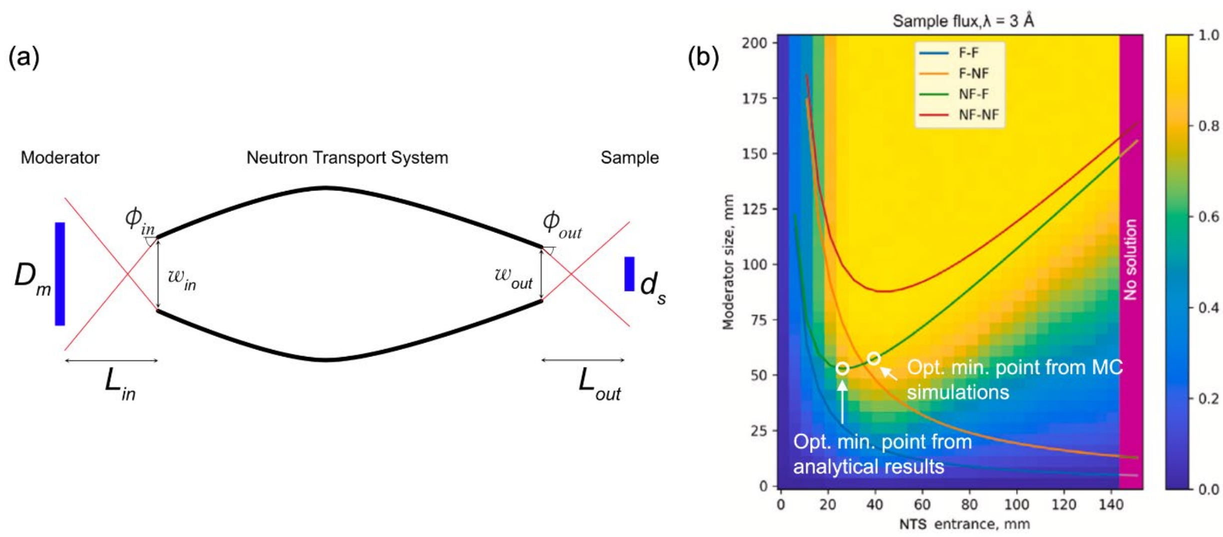

Figure 7: (a) Illustration of a general neutron instrument layout focusing on the main optical components. (b) Sample flux maps from Monte Carlo simulations for λ = 3.2 Å with an elliptical neutron guide. The NTS entrance is the size of the guide entrance W_{in}. The colored lines are the COFSIs for the four extreme cases mentioned in the main text. The envelopes of maximal flux qualitatively agree with the COFSI for the NF–F case when $W_{\text{in}} \gtrsim W_{\text{in\_opt\_min}}$ (green solid line) and disagree with COFSIs for other types; therefore, elliptic guides considered for the simulation are close to the NF–F case. Figures adapted from Ref. [Konik2023].

analytical approach is based on the phase space formalism, essentially identical to the acceptance framework used for the QIKR case; and there is a small correction based on Monto-Carlo simulations.

3.1 CURVES OF OPTIMAL AND FULL SAMPLE ILLUMINATION

Figure 7(a) shows the schematic layout of a general neutron instrument, where D_m and d_s are the source and sample sizes, respectively; L_{in} and L_{out} denote the source-to-guide-entrance and the guide-exit-to-sample distances, respectively; W_{in} and W_{out} are the sizes of the guide entrance and exit, respectively; ϕ_{in} and ϕ_{out} are the neutron beam divergences accepted by the guide entrance and the neutron beam divergence at the guide exit, respectively. These parameters collectively dictate the beam's phase space volumes at both the guide system's entrance and exit.

Konik and Ioffe have formulated the Curves of Optimal and Full Sample Illumination (COFSI) functions, which determine the optimal source size based on these parameters. The point on these curves represents the optimal conditions when the phase space volumes of the beam at the entrance and exit of the guide system are balanced. The specific form of the COFSI curves varies depending on the types of guides employed. Neutron guides can feature either focusing (F) or non-focusing (NF) characteristics at their entrance and exit points. In extreme focusing and non-focusing scenarios, the phase space volumes can be derived analytically at the guide entrance and exit. Four distinct cases are considered: F-F, F-NF, NF-F, and NF-NF, where the first letter(s) denotes the entrance type, and the second letter(s) indicates the exit type. In Fig. 7, the four lines illustrate the outcomes for a typical case utilizing a post-guide Soller or natural collimation system, with d_s = 10 mm, α_s = 1.0°, L_{in} = 2.0 m, and L_{out} = 0.5 m, respectively. Here, α_s represents half of the beam divergence on the sample. Gallmeier et al.'s studies demonstrate that source brilliance increases with decreasing moderator size [Gallmeier2016]. Consequently, for cases featuring a focusing entrance (F-F and F-NF), optimal performance is achieved with the smallest feasible moderators (constrained by engineering), resulting in the highest flux on sample. Conversely, an optimal, minimum moderator size solution exists for cases with a non-focusing entrance (NF-F and NF-NF).

Konik and Ioffe have also conducted Monte-Carlo simulations for a realistic guide system to determine the neutron flux at the sample position for different combinations of (W_{in}, D_m). This analysis involved a 100-meter-long elliptical guide with *m*=3 supermirrors. The results, visualized in the color map of Fig. 7(b), indicate the proximity of the elliptical guide system to the NF-F case. In the extreme NF-F scenario, the COFSI curve is defined as follows,

$$D_{opt} = \frac{2d_s\alpha_s L_{in}}{W_{in}} \quad (8)$$

Here, the optimal moderator size only depends on the product of beam size and divergence, reflecting the requisite phase space volume at the sample location. This characteristic allows for a single optimized moderator size accommodating both high-flux mode with small samples and high-resolution mode with larger samples, facilitating the design of STS instruments to support multiple operational modes. Next, we shall consider the science case requiring maximum phase space volume to estimate the optimal moderator size.

Simulations show two notable differences from the analytical results. First, Monte Carlo simulations unveiled wavelength-dependent outcomes due to imperfect mirror reflection that is ignored in the analytical approach. Secondly, a deviation was observed in the optimal size pair, leaning towards a slightly larger (~112%) moderator and a larger (~160%) guide entrance compared to the analytical results.

3.2 COFSI FOR PIONEER

PIONEER is a single-crystal diffractometer [Liu2022] with a modified elliptical guide. Therefore, we derive the COFSI based on the NF-F scenario. We have considered the configuration for the largest beam size and divergence, indicating the largest phase space volume required by its science case, where d_s = 5 mm and α_s = 0.35°. We use L_{in} = 2.59 m and L_{out} = 1.54 m, optimized from Monte-Carlo simulations tailored to a moderator size of 30 mm. Figure 8 (a) illustrates the computed COFSI, including the parameter pairs selected for PIONEER alongside the minimum moderator case. Note that

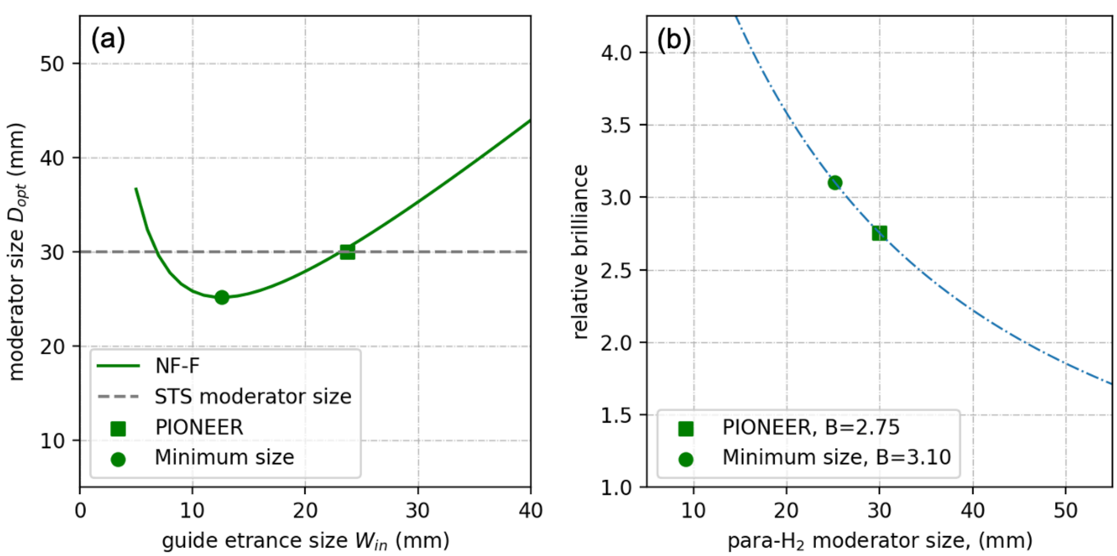

Figure 8: (a) The NF-F COFSI using PIONEER's parameters. Also shown are the ($W_{\text{in\_pioneer}}$, D_{STS}) and (W, $D_{\min}$) pairs, which are the parameters used for POINNER and for the minimum moderator case, respectively. (b) The relative source brilliance as a function of the size of para-H2 moderators.

the parameter pairs chosen for PIONEER align precisely with the COFSI, underscoring the effectiveness of our guide optimization process in identifying the optimal solution.

The analytical determination of the minimum moderator size yields D_{opt} = 25.2 mm, approximately 16% smaller than the moderator size employed for guide optimization. However, this finding is congruent with Konik and Ioffe's Monte Carlo simulations, indicating that a slightly larger moderator can yield higher flux-on-sample, as corroborated in Figure 7(b).

3.3 EFFECT OF MODERATOR SIZE ON PERFORMANCE

Para-H_2 moderators demonstrate a pronounced size-dependent brilliance, with smaller moderators yielding higher brilliance [Gallmeier2016]. Konik and Ioffe have parameterized a function to characterize the dependence of relative brilliance on moderator size [Gallmeier2016]:

$$B(D_m) = \frac{p_1 D_m + p_2}{D_m^2 + q_1 D_m + q_2}, \tag{9}$$

where D_m is measured in centimeters, p_1 = 10.4271, p_2 = 38.3069, q_1 = 3.7588, and q_2 = 4.9990. The relative value is referenced to the case of a 100-mm moderator. This relationship is visualized in Fig. 8(b), indicating that the source brilliance experiences an 11% decline when its size increases from 25.2 mm (the optimal value per the COFSI analysis) to 30.0 mm. However, it is noteworthy that the guide entrance size increases significantly from 12.6 mm to 23.7 mm, leading to a corresponding increase in the guide cross-section. This enlargement of the guide opening proves beneficial in mitigating flux loss due to guide misalignment.

As discussed above, Monte Carlo simulations employing a realistic guide suggest that the optimal moderator size is slightly larger (approximately 12%) than the value determined by the COFSI analysis. Consequently, we infer that a 30-mm moderator is close to the optimal size for PIONEER.

3.4 ABOUT VERDI AND CHESS

VERDI and CHESS will also use quasi-elliptical guides, so we will briefly discuss these two cases here. Equation 8 demonstrates that we can reduce L_{in} if a larger phase space volume is necessary at the sample position to ensure the optimal and full sample illumination for a fixed moderator size. Consistent with STS moderator-area space limitations, we shall keep $L_{in} \gtrsim$ 1.02 m for the cylindrical moderator and $L_{in} \gtrsim$ 0.807 m for the tube moderator. PIONEER employs the cylindrical moderator, with a nearly optimal condition found when L_{in} = 2.59 m for D = 30 mm and d_s = 5 mm, α_s = 0.35°. Consequently, a 30-mm cylindrical moderator can accommodate a maximum phase space volume of approximately 250% of the PIONEER case, while a 30-mm tube moderator can support up to 320% of the PIONEER case.

VERDI is a powder diffractometer [Garlea2022] facing the cylindrical moderator, requiring d_s = 5 mm, α_s = 0.50° for the high-flux mode, and d_s = 10 mm, α_s = 0.15° for the high-resolution mode. The largest phase space volume VERDI requires is 140% of the PIONEER case presented above. Hence, a 30-mm cylindrical moderator suffices for the VERDI science case.

CHESS is a spectrometer [Sala2022] facing the tube moderator, requiring d_s = 20 mm and α_s = 0.6° for high-flux and its largest sample. However, most measurements will use samples much smaller than 10 mm, aligned with the targeted beam size optimized by the guide system. Therefore, the largest phase space volume CHESS requires is 680% (340%) of the PIONEER case for the extreme (practical) case. Although a 30.0-mm tube moderator will not be able to achieve full sample illumination for the extreme cases, it is sufficiently large for most of CHESS's science. Consequently, although a 30-mm tube moderator will not attain the optimal and full sample illumination for extreme cases, it remains sufficiently large for the bulk of CHESS's science applications.

4. THE SUITABILITY OF COMPACT NEUTRON MODERATORS FOR CENTAUR

CENTAUR is a multifunctional high-performance small-angle neutron scattering (SANS) instrument with wide-angle and diffraction capabilities. It will wide Q coverage up to the diffraction region, allowing investigations spanning from atomic to mesoscopic scales simultaneously, with measurement time for structural evolution/change as good as a few seconds for certain systems. With this broad Q coverage, the priority is to design the instrument to ensure a highly collimated beam to achieve the low Q required by SANS. Due to a very broad user community with different sample types ranging from ordered (yet lower order than single crystals especially in the length scales above tens of nanometers) to highly disordered and isotropic samples. The instrument can adjust beam divergence for different SANS experiments. A secondary goal is to expand the Q range to wide-angle and diffraction regions by employing additional detector coverage and the broad natural wavelength band from the source. The collimation for the SANS configuration is always sufficient for diffraction, therefore no additional discussion for diffraction is necessary. The discussion of moderator size is therefore focused on the performance of SANS.

For SANS, sample cross-sectional areas are on the order of 1 cm^2, with smaller sizes desirable. The beam divergence requirement varies depending on cross-sectional area. Typically, an incident divergence of 0.1° or even ~ 1° is useful. Often, limited sample amount/size and the resulting long counting time is the limiting factor for a successful experiment. Usually, divergence is relaxed to improve the flux on the sample, so long as the $Q_{\min}$ needed is attainable with that divergence.

To ensure the sample is fully illuminated, the neutron guide cross-section is designed to be larger than the sample (Fig. 9). The divergence angle θ on sample (Fig. 9) is defined by

$$\cot\theta = \frac{2L_2}{d_g + d_s}. \tag{10}$$

According to [Zhao2013], the guide will be fully illuminated by the moderator if it is placed at an optimal distance L_1'' from it, preferably filling phase space:

$$L_1'' = \frac{1}{2}\left(d_m - d_g\right)\cot\theta. \tag{11}$$

The moderator size satisfying both divergence and illumination can be derived from Eqns.10 and 11:

$$d_m = \left(\frac{L_1''}{L_2} + 1\right)d_g + \frac{L_1''}{L_2}d_s. \tag{12}$$

For CENTAUR, the collimation distance L_2 is adjustable up to 10 m, and the guide to moderator distance can be practically minimized to be ~ 1 m. Therefore, at the smallest divergence, $L_1''/L_2 < 0.1$ in Eqn. 12, the optimal moderator size then should be marginally larger than the guide dimension. For a compact moderator and small guide dimension, assuming further reducing sizes of both presents an engineering challenge, they can be the same size. On the other hand, at the largest divergence, e.g., when L_2 is ~3m, the moderator size needs to be slightly larger than the guide, about 30% to 50% depending on the sample size as more divergence can be utilized by the sample. An overly large moderator is not useful, especially if a more compact moderator will be brighter.

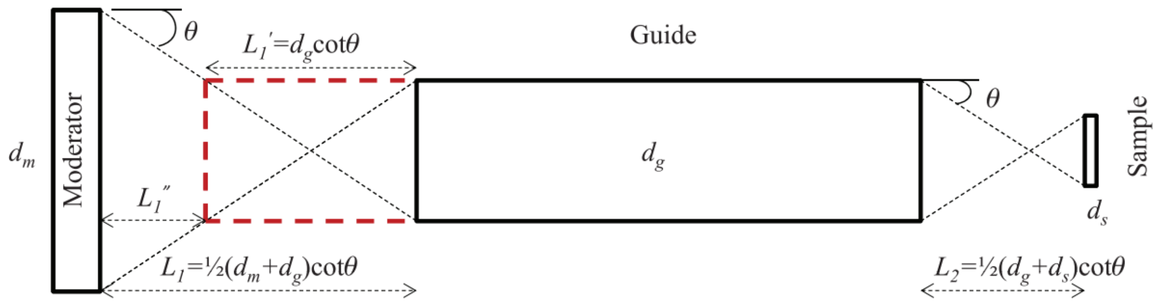

Figure 9: CENTAUR with a straight guide between the moderator and the sample. d_m and d_g are the linear cross-sectional dimensions of the moderator and the neutron guides. The red dashed lines are the optimal guide placement with the guide located L_1'' away from moderator. (Adapted from [Zhao2013]).

The above calculation demonstrates the small moderator with high time-integrated brightness suits CENTAUR best. The longer emission time can be ignored in this discussion. The coupled cold neutron tube moderator with 30 mm diameter matched with straight octagonal guides with 30-mm cross section serves the mission at CENTAUR well. [Qian2024].

5. CONCLUSION

The treatment above demonstrates that the smaller 30×30 mm^2 best serves the scientific mission of QIKR, PIONEER, VERDI, CHESS, and CENTAUR. What about the other instruments in the STS suite? Broadly, the design focus for these instruments [RSI_STS2023] has been to optimize the study of small samples at high resolution and so they have been optimized to make best use of the small, bright STS moderators. Since neutron scattering has traditionally required large sources and beams to make the best use of limited flux, pushing to smaller samples and better resolution best serves the scientific mission of STS. The small, bright moderator enables that mission.

REFERENCES

[Aliakseyeu2023] "Salt-Induced Diffusion of Star and Linear Polyelectrolytes within Multilayer Films", A. Aliakseyeu, P.P. Shah, J.F. Ankner, and S.A. Sukhishvili, Macromolecules 56, 5434 (2023).

[Ankner1992] "Subsurface profile refinement for neutron specular reflectivity", J.F. Ankner and C.F. Majkrzak, in *Neutron Optical Devices and Applications*, SPIE Conference Proceedings, Vol. 1738 (SPIE, Bellingham, Washington, 1992), pp. 260-69.

[Ankner2023] "Cinematic reflectometry using QIKR, the quite intense kinetics reflectometer", J.F. Ankner, et al., Rev. Sci. Instrum. 94, 013302 (2023).

[Browning2019] "Role of conductive binder to direct solid-electrolyte interphase formation over silicon anodes, K.L. Browning, J.F. Browning, M. Doucet, N.L. Yamada, G. Liu, G.M. Veith, Phys. Chem. Chem. Phys. 21, 17356 (2019).

[Carpenter1982] "Neutron Guide Tube Gain for a Remote Finite Source", J.M. Carpenter and D.F.R. Mildner, Nucl. Instrum. and Methods 196, 341 (1982).

[Gallmeier2016] “Conceptual moderator studies for the Spallation Neutron Source short-pulse second target station”, F.X. Gallmeier, W. Lu, B.W. Riemer, J.K. Zhao, K.W. Herwig, and J.L. Robertson, Rev. Sci. Instrum. 87, 063304 (2016).

[Garlea2022] "VERDI: VERsatile DIffractometer with wide-angle polarization analysis for magnetic structure studies in powders and single crystals," Garlea, V. Ovidiu, Stuart Calder, Thomas Huegle, Jiao YY Lin, Fahima Islam, Alexandru Stoica, Van B. Graves, Benjamin Frandsen, and Stephen D. Wilson. Rev. Sci. Instrum. 93, 065103 (2022).

[Liu2022] "PIONEER, a high-resolution single-crystal polarized neutron diffractometer," Liu, Yaohua, Huibo Cao, Stephan Rosenkranz, Matthew Frost, Thomas Huegle, Jiao YY Lin, Peter Torres, Alexandru Stoica, and Bryan C. Chakoumakos, Rev. Sci. Instrum. 93, 073901 (2022).

[Konik2023] "A new method to find out the optimal neutron moderator size based on neutron scattering instrument parameters," Konik, Petr, and Alexander Ioffe, Nucl. Instrum. Methods Phys. Res. 1056, 168643 (2023).

[Phan2020] “X-ray and neutron reflectivity studies of styrene-maleic acid copolymer interactions with galactolipid-containing monolayers”, M.D. Phan., O. Korotych, N.G. Brady, M.M. Davis, S.K. Satija, J.F. Ankner, and B.D. Bruce, Langmuir 36, 3970 (2020).

[Qian2024] S. Qian, C. Boone, F. Ye, Y. Zhang, “Optimization of neutron chopper and optics for CENTAUR, the SANS/WANS diffractometer at the spallation neutron source second target station”, Nuclear Instruments and Methods in Physics Research Section A: Accelerators, Spectrometers, Detectors and Associated Equipment, 169253 (2024).

[RSI_STS2023] https://pubs.aip.org/collection/1617/New-Science-Opportunities-at-the-Spallation, accessed 15 March 2024.

[Sala2022] "CHESS: The future direct geometry spectrometer at the second target station," Sala, G. et al., Rev. Sci. Instrum. 93, 065109 (2022)

[Zhao2013] “Optimizing moderator dimensions for neutron scattering at the spallation neutron source”, J.K. Zhao, J.L. Robertson, Kenneth W. Herwig, Franz X. Gallmeier, and Bernard W. Riemer, Rev. Sci. Instrum. 84, 125104 (2013).

APPENDIX A. ADD TITLE FOR APPENDIX A

APPENDIX A. TITLE